Flow structure generated from an axisymmetric natural air jet at a moderate Reynolds number

Yassine Zaouali, Taoufik Filali, Habib Ben Aissia, Jacques Jay

FDR385884 on 14 March 2011

IOP PUBLISHING FLUID *DYNAMICS* RESEARCH

Fluid Dyn. Res. **73** (2011) 000000 (13pp) UNCORRECTED PROOF

Flow structure generated from an axisymmetric natural air jet at a moderate Reynolds number

Yassine Zaouali[1], Taoufik Filali[1], Habib Ben Aissia[1] and Jacques Jay[2]

[1] Unit of Metrology in Fluid Mechanics and Thermal (03/UR/11-09), National School of Engineering of Monastir, Avenue Ibn Eljazzar, 5019 Monastir, Tunisia
[2] Thermal Centre of Lyon (CETHIL—UMR CNRS 5008), National Institute of Applied Sciences of Lyon, 9 rue de la physique, 69621 Villeurbanne Cedex, France

E-mail: yes.zaouali@laposte.net

Q1

Received 2 August 2010, in final form 16 February 2011
Published xxx
Online at stacks.iop.org/FDR/73/000000

Communicated by A Gilbert

Abstract

This paper reports on an experimental study of a free air jet evolving naturally and discharging from a round nozzle at a Reynolds number of 1600. By using flow visualization images and time-series analysis, the details of the flow behavior are clarified. In particular, the length of the transition zone of the jet is measured and its temporal evolution is investigated. We show that the vortex structures interact with each other, thus producing different sizes in the flow. The probability distribution and temporal evolution of the jet width at various distances from the nozzle exit are studied. The occurrence frequency of vortex rings and the Strouhal number of the jet were also determined at different positions from the nozzle exit. The results obtained are compared with those reported in the literature.

(Some figures in this article are in colour only in the electronic version)

1. Introduction

In modern technology, air jets are widely used in diverse applications, particularly in the drying process, thermal insulation using an air curtain, cooling of electronic components, etc. The free jet is also an important flow field as it includes several phenomena concerning instabilities formation (Kelvin–Helmholtz), vorticity separation and roll up into vortices, vortex pairing, free turbulence evolution and viscous/inviscid interactions (Becker and Massaro 1968, Crow and Champagne 1971, Hussain and Zaman 1980, Cantwell 1981, Chao *et al* 1990).

Therefore, free jets evolving at diverse Reynolds numbers are still open topics of research, and the specific literature is consequently rich and varied (Xu and Antonia 2002,

Q2

0169-5983/11/010000+13$33.00

O'Neill *et al* 2004, Zaouali *et al* 2004, 2009, 2010, Kwon and Seo 2005, Nastase *et al* 2008, Shinneeb *et al* 2008, Todde *et al* 2009, Hassan and Meslem 2010).

From an experimental standpoint, free round jets have been studied for both low and moderate Reynolds numbers, especially in natural conditions. In this case, a number of experimental studies have been conducted to investigate the onset of instabilities and growth of structures in the jet shear layer (Reynolds 1962, Viilu 1962, Crow and Champagne 1971, Mattingly and Chang 1974). The consistent findings of these various experimental studies were that the Reynolds number is a pertinent parameter for determining the mode of instability, and as the Reynolds number increases the instability mode changes from helical to axisymmetric. In fact, two distinct geometric instabilities have been observed: axisymmetric, where the jet appears to pulsate, and helical, where the jet appears to undulate rhythmically (Crow and Champagne 1971).

The occurrence of both axisymmetric and helical modes of instability at low and moderate Reynolds numbers has also been reported in theoretical studies (Batchelor and Gill 1962, Crow and Champagne 1971, Mattingly and Chang 1974, Cohen and Wygnanski 1987, Danaila *et al* 1997).

For jets at high Reynolds numbers, the distance from the exit section required for the instabilities formation is very small, and the evolution of the vortices is faster. Therefore, the instabilities are not observable at all due to their very fast decay.

From a technical and instrumental standpoint, experimental investigations of low- and moderate-Reynolds-number round jets mostly use flow visualization methods to qualitatively identify instabilities. O'Neill *et al* (2004) compared the behavior of round water jets with two Reynolds numbers of 680 and 1030 near the orifice region from 2 to 14.4 diameters using the particle image velocimetry (PIV) technique. It was found that the jet is marginally unstable at a Reynolds number of 680, whereas at a Reynolds number of 1030 the jet is manifestly unstable close to the orifice and laminar-to-turbulent transition follows with the jet approaching self-similar turbulent behavior further downstream. Kwon and Seo (2005) conducted experiments for jets discharging from a round contraction nozzle in order to gain a better understanding of the behavior of the non-buoyant round water jet for a wide range of Reynolds numbers (from 177 to 5142). In this study, a PIV system was used to measure the cross-sectional velocity distributions, and instantaneous images showing the evolution of the round jet with increasing Reynolds number are presented. The images show that the laminar, transitional and turbulent flows can coexist in a circular jet with sufficient longitudinal distance. It can be clearly seen that the axial length of the laminar or transitional region prior to the turbulent flow decreases with increasing Reynolds number. Nastase *et al* (2008) associated PIV measurements and high-speed visualizations enriched by low-level image processing, for the analysis of the vortical dynamics in the near field of an air jet flow with a Reynolds number of 813. These authors are particularly interested in the contribution of vortical structures to the entrainment process of low-Reynolds-number jet flows. They show that, in the round jet, the entrainment is produced in the braid region (region between two successive rings), where streamwise structures develop. In the Kelvin–Helmholtz ring, entrainment is dramatically affected by the attenuation of the streamwise structures. Todde *et al* (2009) presented hot-wire measurements along the centerline of a jet issued from an orifice with a diameter of 0.040 m and nominal outlet speeds ranging from 0.30 to 2.50 m s^{-1}, giving thus a Reynolds number (Re) based on the diameter, in the range of $850 \leqslant Re \leqslant 6800$. The results showed evidence of several flow regimes in the range of Reynolds number examined; in particular, a first regime appears to include the flows at Reynolds numbers up to about 1600. In this regime, the flow is essentially laminar and dissipation of energy is quite weak. Moreover, an alternation between helical and azimuthal

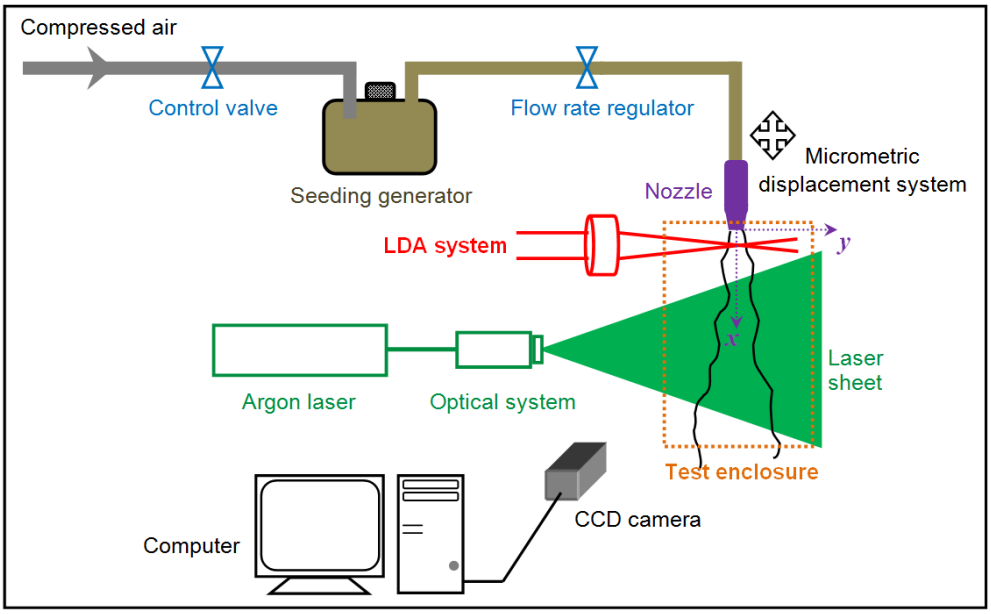

Figure 1. The experimental setup.

instabilities of the jet column was hypothesized to be the mechanism leading to vortex generation.

Among the works concerning the behavior of round jets, very few studies were devoted to the spatiotemporal dynamics of instabilities that occur in air jet flows with low and moderate Reynolds numbers.

In this study, therefore, laboratory experiments for a jet discharging from a round nozzle were conducted in order to gain a better understanding of the spatiotemporal evolution of the instabilities in an air jet. In our experimental study, we were particularly interested in the development of the axisymmetric Kelvin–Helmholtz instability (the varicose mode) obtained, in our case, for a Reynolds number of 1600. Using flow visualization images and time-series analysis, we investigated the flow structure of a round jet, the formation process of vortex rings and the probability distribution of the jet width of flow included in the jet at various axial positions from the nozzle exit. The occurrence frequency of vortex rings and the Strouhal number of the jet are also measured.

2. Experimental setup and jet exit conditions

In this experiment, the free air jet is generated by a nozzle of 12.4 mm internal diameter (D) discharging into ambient air. The nozzle is at a height of 2 m above the ground. The essential features of the experimental setup are schematically shown in figure 1. It should be noted that in this paper, the origin of the coordinate system used is at the centre of the jet exit with the x-axis extending in the axial direction. Although this is a round jet, measurements will be reported on a Cartesian measurement plane (x and y) that includes the jet axis.

The compressed air goes through a series of flow rate regulators and is seeded by micrometric incense smoke particles generated in the upstream circuit. Arriving at the nozzle, it crosses successively a honeycomb, three fine grids and exhausts from an axisymmetric

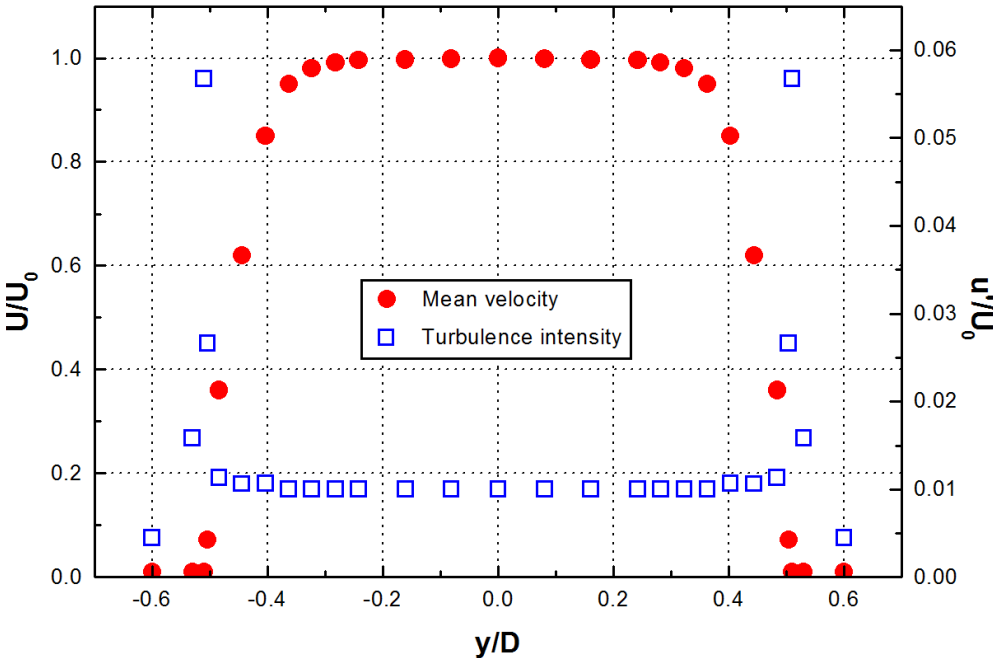

Figure 2. Nozzle exit: mean velocity and turbulence intensity profiles; $Re = 1600$; distance from the nozzle exit $x/D \approx 0.16$.

convergent nozzle correctly profiled, in order to reduce the turbulence level. The resulting vertical jet is centered in a 0.40 (length) × 0.40 (width) × 1.5 (height) m^3 Plexiglas cell with an open outlet, in order to isolate the jet from external disturbances as much as possible. A light sheet, produced by sending the beam generated by a 7 W argon laser source through a cylindrical lens, illuminates the central section of the jet in the vertical plane in a region extending up to $x/D \approx 10.0$, where x is the axial coordinate. The visualization is done by heavily seeding the jet fluid with particles and acquiring images during the time when the seeded jet first enters the unseeded ambient fluid. Images of the jet are captured with a fast digital camera (maximum cadency of 220 images s^{-1} and maximum resolution of 1300 × 1030 pixels) connected to a PC in order to store several sequences per experiment (300 images per sequence). Thus the images obtained show a satisfactory freezing of the situation, allowing the identification of the expected phenomena.

On the other hand, measurements of the jet velocity profile at the nozzle exit and the turbulence statistics were obtained using a laser Doppler anemometer (LDA) in forward scatter configuration made by Dantec (Ben Aissia 2002, Kechiche *et al* 2009).

Throughout this experiment, the jet exit velocity is fixed at $U_0 = 2.0\,m\,s^{-1}$ and is verified by the LDA system. The corresponding Reynolds number based on the nozzle exit diameter (D) and the kinematic viscosity (ν), $Re = U_0 D/\nu$, is 1600.

The outflow conditions in the jet cross-section were checked 2.0 mm downstream of the exit section; typical normalized profiles of mean velocity (U/U_0) and turbulence intensity (u'/U_0) are shown in figure 2. In this figure, y represents the radial coordinate. However, it can be seen that the mean velocity profile has a satisfactorily sharp top-hat shape. The fluctuation intensity profile shows a very low value (≈ 1%) throughout the constant-velocity region of the jet section. On the sides, where the velocity reduction is observed, u'/U_0 slightly

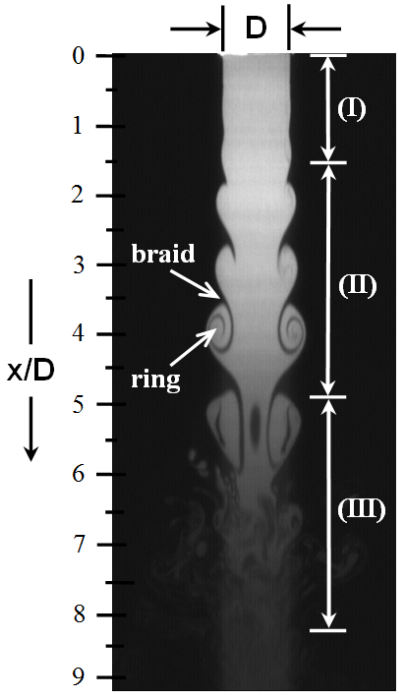

Figure 3. Jet flow visualization; $Re = 1600$. (I) Vortex rollup, (II) vortex region and (III) vortex breakdown.

increases to a maximum of about 6%. This moderate turbulence intensity value confirms the laminar nature of the exit boundary layer. Finally, a satisfactory symmetry exists between the two sides of the jet, which is clearly observable in both profiles.

3. Results and discussions

3.1. Flow visualization

Figure 3 reports a visualization from the present work in which several vortical structures can be identified together with the subsequent decay. In this figure, it is possible to observe the first region of the jet characterized by a short laminar zone followed by very weak undulation, which quickly generates a discrete vortex (I). The second region constitutes a zone of evolution of successive vortices moving downstream within the shear layer and growing in size (II) to end finally in a zone of chaos and disorder where the vortical structures disappear completely in the core closure (III).

In figure 4, we report two visualizations that illustrate the most important phenomena that were observed. This figure displays two images of the jet at different time instants (the time interval between the two images is approximately 0.08 s). In both cases, it seems that a roll-up of the shear layer into vortical structures has occurred, and the resulting structures are symmetric on both sides of the jet axis and appear to grow as the flow proceeds downstream.

However, two different topologies are present in the field: in figure 4(a), all the vortices are neatly separated and no evidence of interaction can be observed, while in figure 4(b) an ongoing vortex pairing between the vortices at $4.0 < x/D < 5.5$ is evident (the one more downstream appears to be absorbing the other one).

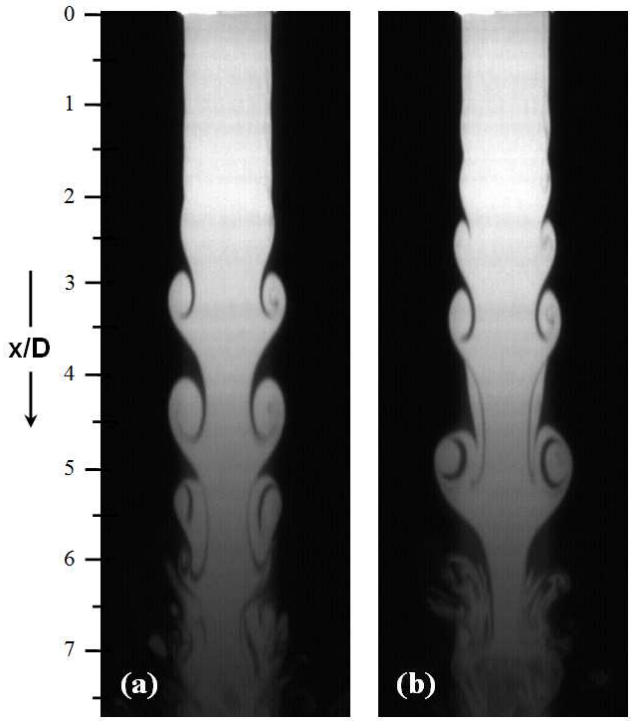

Figure 4. Flow visualization: two separate realizations ($Re = 1600$; $\Delta t = 0.08$ s).

In fact, for this range of Reynolds number, the pairings were quite difficult to observe. This was attributed to the very low speed of the vortices, which makes their interaction slow and hardly observable. When the Reynolds number is increased, this interaction becomes much more evident.

3.2. Vortex initiation distance and vortex breakup location

This section describes the transition zone of the flow, where the Kelvin–Helmholtz instability originates and develops in the form of vortex structures. Several sequences of 300 images of the jet are recorded with a time interval equal to 1/220 s and then treated. An example of these images is presented in figure 5(a). The treatment objective is to detect the jet edges. For this, a binarization of the original images is obtained through a threshold procedure based on a Sobel algorithm (Nixon and Aguado 2002). As shown in figure 5(b), the images are transformed so that the flow region becomes white and its ambiance becomes black. The transition between black and white regions is then located by detecting pixels that have large variation of intensity gradient in order to draw the corresponding contour (figure 5(c)).

Vortex initiation distance (x_i) is defined as the distance from the jet exit where the instability that causes vortex formation is first observed. This instability wave grows and eventually rolls up into a vortex. Vortex breakup location (x_b) is the location where the core of the vortex begins to exhibit instability, rather than coherent vortex motion (see figure 5). Thus, the extent of each distance x_i and x_b is observed and identified on all the recorded images of the sequence, with a maximum uncertainty of 2 pixels. The probability distribution of x_i and x_b, scaled in diameters from the jet exit, is shown in figure 6.

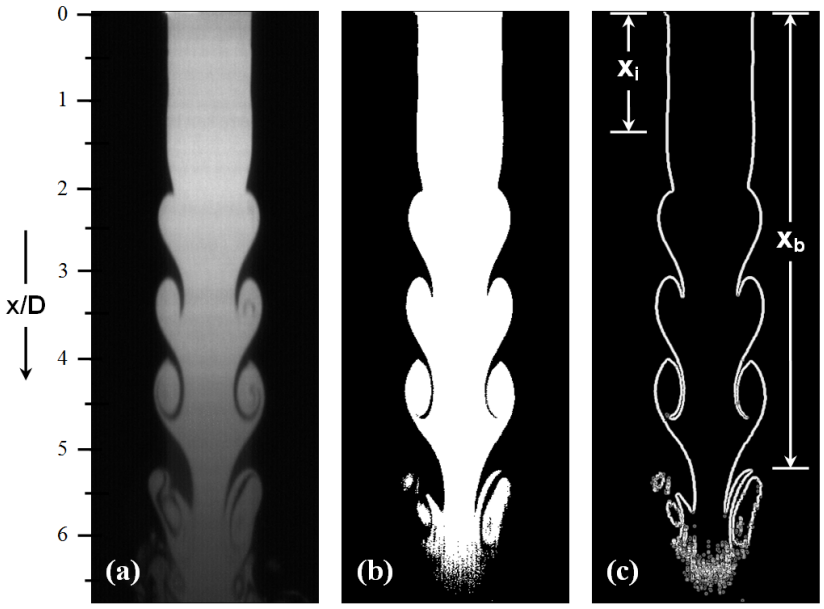

Figure 5. Definition of the measured parameters and edge detection images. (a) Original image, (b) thresholded image and (c) identifier contour.

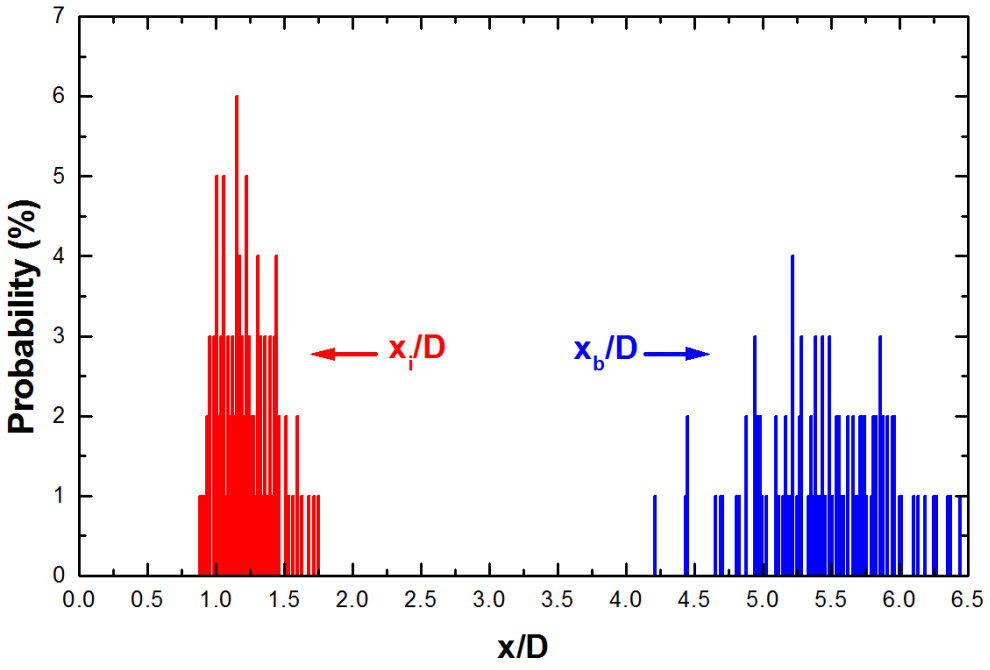

Figure 6. Probability distribution of vortex initiation distance (x_i/D) and vortex breakup location (x_b/D).

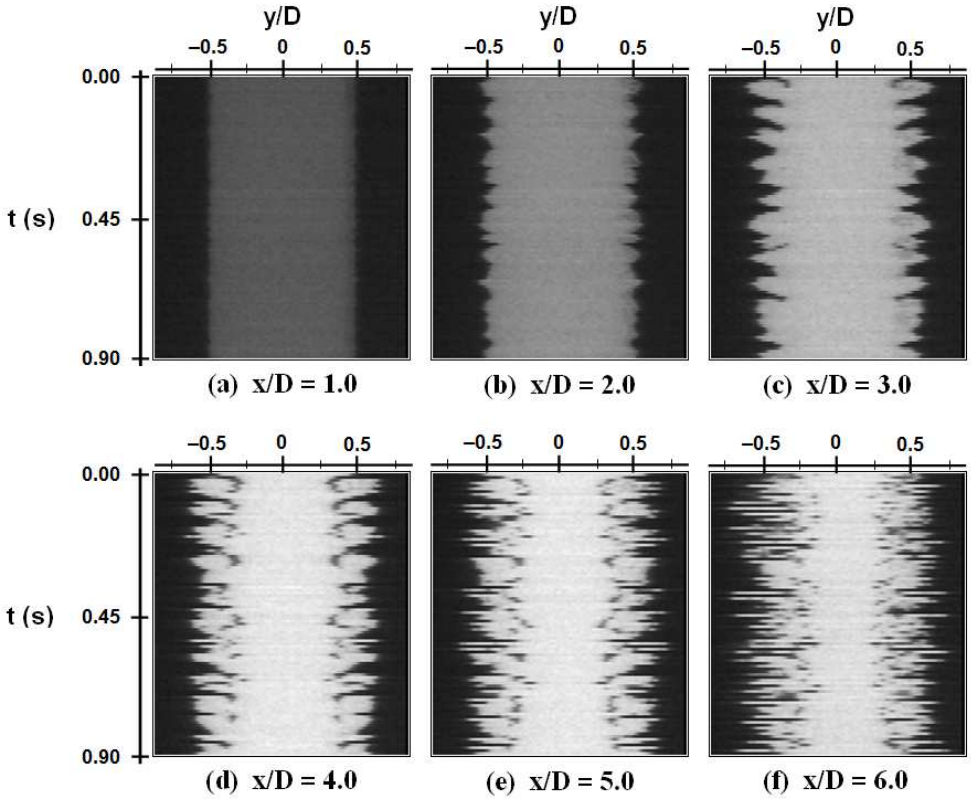

Figure 7. Flow visualization of time-series analysis of the jet ($Re = 1600$; $\Delta t = 1/110$ s).

In the case of $Re = 1600$, the average value of x_i is estimated to be 1.22 diameters, with a standard deviation of the distribution equal to 0.20 ($\approx 16\%$). The vortex breakup location (x_b) is found to be 5.45 diameters, with a standard deviation equal to 0.46 ($\approx 8\%$). Knowing the extent of the potential core, which is of order of 5–6 diameters of the nozzle exit in this range of Reynolds numbers (Zaouali *et al* 2010), we can deduce that the vortex breakup location is related to the end of the potential core in our case. On the other hand, the length of the jet transition zone, defined here by $(x_b–x_i)/D$, is also determined. The average value of $(x_b–x_i)$ is found to be 4.23 diameters, with a standard deviation equal to 0.42 ($\approx 10\%$).

From these values, it is evident that the vortex initiation distance x_i and the vortex breakup location x_b are not stable in time. Thus, we can predict that a global vertical movement of the jet is present in the flow. This implies that the potential core is not a continuous phenomenon in time.

3.3. Time-series analysis

Figures 7(a)–(f) show the results of a time-series analysis at $x/D = 1.0$, 2.0, 3.0, 4.0, 5.0 and 6.0, respectively. The various spatiotemporal diagrams presented here are built using horizontal lines extracted from the images of the jet with 110 frames per second. Thus, it is possible to follow the temporal evolution of the width of flow included in the jet at the various sections.

Figure 7(a) shows the image of the instantaneous width of the flow at $x/D = 1.0$ during 0.90 s. It can be seen that the jet size is maintained at about $y/D = \pm 0.5$. The flow behavior is as a mass of almost identical size; the vortex rings are not yet formed.

Figure 7(b) also shows the image of the jet width at $x/D = 2.0$. A slight jet width variation from $y/D = \pm 0.5$ is visible on the diagram. This indicates the beginning of the appearance of small-sized vortex rings in this axial position of the jet.

At $x/D = 3.0$ (figure 7(c)), the smaller vortex rings have grown in size and the jet width varies considerably from the nozzle limits. Two different sizes then begin to appear in the structure of the jet.

Further downstream, as shown in figure 7(d) for $x/D = 4.0$, the jet enlarges even more. In fact, the smaller vortex rings, having faster velocity than the larger one, catch up these last ones. The smaller vortex rings are then absorbed by the larger ones. These vortical structures then begin to separate from the rest of the flow, whose central part becomes smaller.

This separation becomes more visible on figure 7(e), at $x/D = 5.0$, where some vortical structures begin to detach from the jet and the general structure of the flow turns out to be disorganized.

As shown in figure 7(f), the jet width at $x/D = 6.0$ varies between $y/D \approx 0.75$ and -0.75. The width of the central part of the jet does not exceed $y/D = \pm 0.25$. Most of the vortex rings become larger and more diffusible. Thus, the jet tends to a transition to turbulence.

In figure 7, the time-series analysis of the jet width shows that just behind the nozzle, the jet has a uniform structure and the existence of the vortex rings is not evident. Further downstream, as x/D increases, vortex rings appear and have several sizes by combining with each other.

3.4. Probability distribution of the jet width

Figure 8 describes the relationship between the width of flow included in the jet (L) and the probability distribution at each position of $x/D = 1.0$, 2.0, 3.0, 4.0, 5.0 and 6.0. In this graph, the jet width is measured for each period of $\Delta t = 1/220$ s and it is non-dimensionalized to the diameter D of the nozzle exit. We use the time-series analysis of the jet presented in figure 7 for this distribution. The images of the instantaneous width of the flow in figure 7 represent the real size of these structures. Therefore, the width of the flow (L/D) is defined as the difference between the positions of the left and right edges of these images.

From these images, it is evident that the width of the probability distribution increases with decreasing the value of the maximum.

In figure 8, the probability distribution at $x/D = 1.0$ presents a single peak showing that the width of the jet is almost the same in this section ($L/D = 1.0$). From the nozzle exit up to this section, no remarkable variation of the structure of the jet is detected.

At $x/D = 2.0$, a peak value corresponding to a probability distribution of 70% is observed. Most of the measured widths are of the order of $L/D \approx 1.0$. Other jet widths having values in the range of $L/D \approx 0.9$–1.1 begin to appear in the flow. The values of $L/D > 1$ for a given axial position correspond to vortex rings, while the values of $L/D < 1$ correspond to braid regions (see figure 3). As was demonstrated by Nastase *et al* (2008), the entrainment then begins to occur in the braid region at this section of the jet. Q3

At $x/D = 3.0$, the width of the probability distribution increases further, and larger sizes begin to appear in the flow. The width of rings varies until $L/D \approx 1.2$ with a peak of 33% at $L/D \approx 1.1$. At this section also, the width of braids decreases and reaches $L/D \approx 0.8$.

Concerning the probability distribution at $x/D = 4.0$, the jet width varies from $L/D \approx 0.7$ to $L/D \approx 1.3$. Most ring widths are of the order of $L/D \approx 1.1$ to 1.2. Meanwhile, the

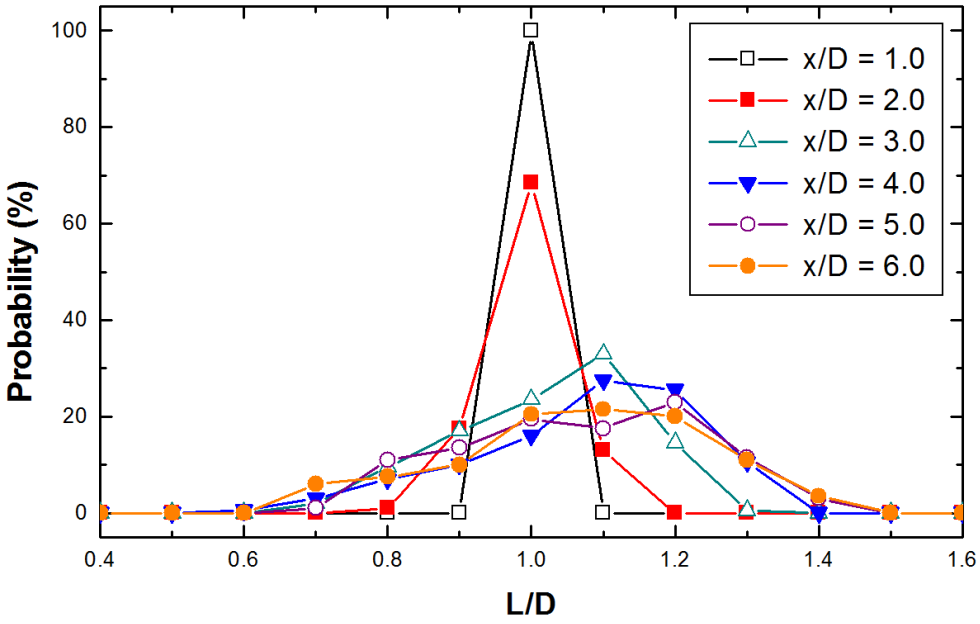

Figure 8. Probability distribution of the jet width at discrete positions from $x/D = 1.0$ to $x/D = 6.0$.

braid width decreases further until reaching the value of $L/D \approx 0.6$. This decrease of the braid width with the axial distance from the nozzle exit is related to the reduction of the potential core size.

Larger vortex rings ($L/D \approx 1.4$) are also observed at $x/D = 5.0$. The evolution of the width of rings shows a continuous increase along the axial distance of the jet, the flow expands.

Q4

At $x/D = 6.0$, the width of the distribution becomes large and it spreads over the range of the jet widths. A slight difference in probability distribution is observed for diverse values of L/D. The jet expands more and more with the end of the potential core region.

Q5

3.5. Frequency and Strouhal number of vortex rings

In this section, the occurrence frequency (F) of the jet vortex rings discharging from the circular nozzle is studied for various discrete positions $x/D = 1.0$, 2.0, 3.0, 4.0, 5.0 and 6.0.

For this, graphs of the temporal evolution of the jet width are plotted for the range of axial distances considered here. An example of these graphs is shown in figure 9(a) obtained for $x/D = 4.0$, during a period of 0.90 s. It can be seen from this figure that the oscillations of the jet width in time show a quasi-periodic passage of vortex rings ($L/D > 1$) at this axial position of the flow.

It should be noted that, using the relationship established by Zaouali *et al* (2010), which gives the convective velocity U_C of vortex rings on the jet edge ($U_C = 0.65U_0$), the average displacement of the ring structures is about $D/2$ during $\Delta t = 1/220$ s. This excludes the passage of several vortex rings at a given axial position for this time interval.

For determining the occurrence frequency of the vortex rings, fast Fourier transform (FFT) of the jet width oscillations for each x/D has been carried out. The corresponding frequency spectra in the case of $x/D = 4.0$ is also presented in figure 9(b). The FFT shows that

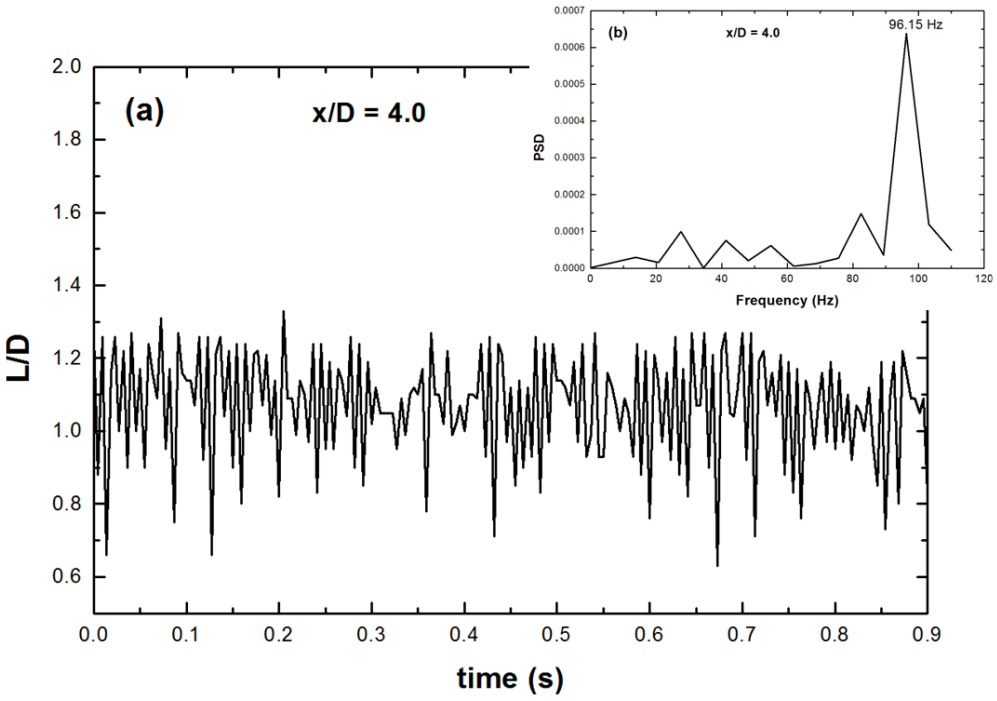

Figure 9. Temporal evolution of the jet width (a) and FFT analysis of the oscillations (b) at $x/D = 4.0$.

Table 1. The frequency and the Strouhal number of vortex rings.

x/D	*F* (Hz)	*St*
1.0	–	–
2.0	98.54	0.61
3.0	98.52	0.61
4.0	96.15	0.60
5.0	87.13	0.54
6.0	49.74	0.31

the dominant frequency is around 96 Hz for the case considered. The occurrence frequency concerning the other axial distances is presented in table 1.

The Strouhal number, defined by $St = \mathrm{FD}/U_0$, is also presented in table 1 for the various axial distances x/D. According to these values, the frequency F and the Strouhal number St decrease gradually with increasing distance from the nozzle exit. However, in the region $2.0 \leqslant x/D \leqslant 4.0$, we found the highest occurrence frequencies of vortex rings ($F \approx 98$ Hz), with an average Strouhal number close to 0.60.

The Strouhal numbers of these jet vortex rings obtained in our case are in the range of 0.31–0.61. These values are in good agreement with the results reported by Gutmark and Ho (1983). In this paper, most of the results concerning the frequency and Strouhal number of the preferred mode of instability were collected for different jet configurations. The authors note that the Strouhal number varies in the range of 0.24–0.64.

4. Conclusion

This experimental work presents the characteristics of an air jet evolving naturally from a circular orifice at $Re = 1600$. The jet behavior was observed by flow smoke visualization Q6 recorded by a high-speed camera with 220 frames per second. On the acquired images, it was possible to identify and to follow the temporal evolution of the structures (vortex rings and braid regions) that appear on the edges of such flows. The measurements of the length of the jet transition zone furnish a value equal to 4.23 diameters with a variation around 10% in time, and that the vortex breakup location is related to the end of the potential core extent.

A time-series analysis of the images at different axial positions from the nozzle exit was also conducted. The probability distribution and the temporal variation of the jet width were investigated. The experimental results show the following:

- Just behind the nozzle, the jet has a uniform structure and the existence of the vortex rings is not evident.
- Further downstream, the vortex rings develop and increase in size. In their growth process, the ring structures remain attached to the central part of the jet while the potential Q7 core exists. The connection between the vortex rings is then broken and the vortices are separated from the rest of the jet at the end of the potential core extent.
- The distribution of the jet width varies considerably according to the distance from the nozzle exit. One size of structures exists just at the jet exit. Further downstream, several vortex rings having different sizes and almost equal distributions appear in the flow, producing a variable distribution of the jet width.

Finally, the occurrence frequency of vortex rings and the Strouhal number of the jet were measured. The results indicate a decrease of the frequency and the Strouhal number with increasing distance from the nozzle exit. However, in the region $2.0 \leqslant x/D \leqslant 4.0$, we found the highest occurrence frequencies of vortex rings ($F \approx 98$ Hz): with an average Strouhal number close to 0.60. These values are in good agreement with those available in the literature.

Acknowledgments

We thank Dr Amina Meslem (LEPTIAB, University of La Rochelle, France) for her careful review of a draft of this paper. This work is dedicated to the martyrs of the Tunisian revolution.

Q8 References

[1] Batchelor G K and Gill A E 1962 Analysis of the instability of axisymmetric jets *J. Fluid Mech.* **14** 529–51

[2] Becker H A and Massaro T A 1968 Vortex evolution in a round jet *J. Fluid Mech.* **31** 435–48

[3] Ben Aissia H 2002 Etude numérique et expérimentale par imagerie et Anémométrie Laser Doppler d'un jet axisymétrique Doctoral Thesis University of Tunis-Elmanar, Tunisia

[4] Cantwell B J 1981 Transition in the axisymmetric jet *J. Fluid Mech.* **104** 369–86

[5] Chao Y C, Han J M and Jeng M S 1990 A quantitative laser sheet image processing method for the study of the coherent structure of a circular jet flow *Exp. Fluids* **9** 323–32

[6] Cohen J and Wygnanski I 1987 The evolution of instabilities in the axisymmetric jet. Part 1. The linear growth of disturbances near the nozzle *J. Fluid Mech.* **176** 191–219

[7] Crow S C and Champagne F H 1971 Orderly structure in jet turbulence *J. Fluid Mech.* **43** 547–91
[8] Danaila I, Dusek J and Anselmet F 1997 Coherent structures in a round, spatially evolving, unforced, homogeneous jet at low Reynolds numbers *Phys. Fluids* **9** 3323–42
[9] El Hassan M and Meslem A 2010 Time-resolved stereoscopic particle image velocimetry investigation of the entrainment in the near field of circular and daisy-shaped orifice jets *Phys. Fluids* **22** 035107
[10] Gutmark E J and Ho C-M 1983 Preferred modes and the spreading rates of jets. *Phys. Fluids* **26** 2932–8
[11] Hussain A K M F and Zaman K B M Q 1980 Vortex pairing in a circular jet under controlled excitation. Part 2. Coherent structure dynamics *J. Fluid Mech.* **101** 493–544
[12] Kechiche N, Abbassi A, Filali T, Jay J and Ben Aissia H 2009 Spectral analysis of round jet instabilities at low Reynolds number *Mech. Ind.* **10** 447–54
[13] Kwon S J and Seo W 2005 Reynolds number effects on the behavior of a non-buoyant round jet *Exp. Fluids* **38** 801–12
[14] Mattingly G E and Chang C C 1974 Unstable waves on an axisymmetric jet column *J. Fluid Mech.* **65** 541–61
[15] Nastase I, Meslem A and Gervais P 2008 Primary and secondary vortical structures contribution in the entrainment of low Reynolds number jet flows *Exp. Fluids* **44** 1027–33
[16] Nixon M and Aguado A *Feature Extraction and Image Processing* (Oxford: Newnes)
[17] O'Neill P, Soria J and Honnery D 2004 The stability of low Reynolds number round jets *Exp. Fluids* **36** 473–83
[18] Reynolds A J 1962 Observations of a liquid-into-liquid jet *J. Fluid Mech.* **14** 552–6
[19] Shinneeb A-M, Bugg J D and Balachandar R 2008 Quantitative investigation of vortical structures in the near-exit region of an axisymmetric turbulent jet *J. Turbul.* **9** 1–20
[20] Todde V, Spazzini P G and Sandberg M 2009 Experimental analysis of low-Reynolds number free jets: evolution along the jet centerline and Reynolds number effects *Exp. Fluids* **47** 279–94
[21] Viilu A 1962 An experimental determination of the minimum Reynolds number for instability in a free jet *J. Appl. Mech.* **29** 506–8
[22] Xu G and Antonia R A 2002 Effect of different initial conditions on a turbulent round free jet *Exp. Fluids* **33** 677–83
[23] Zaouali Y, Ben Aissia, Kechiche N, Jay J and Schon J-P 2004 Experimental study of the instabilities in the laminar turbulent transition zone of an axisymmetric jet at low Reynolds number *J. Flow Vis. Image Process.* **11** 207–22
[24] Zaouali Y, Jay J and Ben Aissia H 2009 Visualization and experimental measures in a round jet evolving at moderate Reynolds number *Mech. Ind.* **10** 437–46
[25] Zaouali Y, Ammar S, Kechiche N, Jay J and Ben Aissia H 2010 Experimental and quantitative investigation of a free round jet *Eur. Phys. J. Appl. Phys.* **52** 11302

QUERY FORM

JOURNAL: fdr

AUTHOR: Y Zaouali *et al*

TITLE: Flow structure generated from an axisymmetric natural air jet

ARTICLE ID: fdr385884

Page 1

Q1.
Please verify the changes made to affiliation no. 1 of the 'Author affiliations' section. Also, check the word 'Thermal'.

Q2.
Verify the changes made to the sentence 'Therefore, free jets evolving at diverse Reynolds numbers are still open topics . . . Hassan and Meslem 2010)'.

Page 9

Q3.
Verify the changes made to the sentence 'The values of $L/D > 1$ for a given axial position correspond to vortex . . . (see figure 3)'.

Page 10

Q4.
Check the sentence 'The evolution . . . flow expands' as it appears to be incomplete.

Q5.
Check 'end' in the sentence 'The jet expands . . . region'.

Page 12

Q6.
Verify the changes made to the sentence 'The jet behavior was observed by flow smoke visualization recorded by a high-speed camera with 220 frames per second'.

Q7.
Check 'exists' in the sentence 'In their growth process, . . . core exists' as the sense is not clear. Check 'extent' in the sentence 'The connection between . . . core extent'.

Q8.
Please check the details for any journal references that do not have a blue link as they may contain some incorrect information. Pale purple links are used for references to arXiv e-prints.

Author: please be aware that the colour figures in this article will only appear in colour in the Web version. If you require colour in the printed journal and have not previously arranged it, please contact the Production Editor now.